Atmos. Meas. Tech., 9, 1431–1447, 2016
www.atmos-meas-tech.net/9/1431/2016/
doi:10.5194/amt-9-1431-2016

Atmospheric Measurement Techniques
Open Access
EGU

Investigation of potential interferences in the detection of atmospheric RO_x radicals by laser-induced fluorescence under dark conditions

Hendrik Fuchs[1], Zhaofeng Tan[2], Andreas Hofzumahaus[1], Sebastian Broch[1], Hans-Peter Dorn[1], Frank Holland[1], Christopher Künstler[1], Sebastian Gomm[1], Franz Rohrer[1], Stephanie Schrade[1], Ralf Tillmann[1], and Andreas Wahner[1]

[1]Institute of Energy and Climate Research, IEK-8: Troposphere, Forschungszentrum Jülich GmbH, Jülich, Germany
[2]College of Environmental Sciences and Engineering, Peking University, Beijing, China

Correspondence to: Hendrik Fuchs (h.fuchs@fz-juelich.de)

Received: 11 November 2015 – Published in Atmos. Meas. Tech. Discuss.: 30 November 2015
Revised: 1 March 2016 – Accepted: 23 March 2016 – Published: 4 April 2016

Abstract. Direct detection of highly reactive, atmospheric hydroxyl radicals (OH) is widely accomplished by laser-induced fluorescence (LIF) instruments. The technique is also suitable for the indirect measurement of HO_2 and RO_2 peroxy radicals by chemical conversion to OH. It requires sampling of ambient air into a low-pressure cell, where OH fluorescence is detected after excitation by 308 nm laser radiation. Although the residence time of air inside the fluorescence cell is typically only on the order of milliseconds, there is potential that additional OH is internally produced, which would artificially increase the measured OH concentration. Here, we present experimental studies investigating potential interferences in the detection of OH and peroxy radicals for the LIF instruments of Forschungszentrum Jülich for nighttime conditions. For laboratory experiments, the inlet of the instrument was over flowed by excess synthetic air containing one or more reactants. In order to distinguish between OH produced by reactions upstream of the inlet and artificial signals produced inside the instrument, a chemical titration for OH was applied. Additional experiments were performed in the simulation chamber SAPHIR where simultaneous measurements by an open-path differential optical absorption spectrometer (DOAS) served as reference for OH to quantify potential artifacts in the LIF instrument. Experiments included the investigation of potential interferences related to the nitrate radical (NO_3, N_2O_5), related to the ozonolysis of alkenes (ethene, propene, 1-butene, 2,3-dimethyl-2-butene, α-pinene, limonene, isoprene), and the laser photolysis of acetone. Experiments studying the laser photolysis of acetone yield OH signals in the fluorescence cell, which are equivalent to 0.05×10^6 cm^{-3} OH for a mixing ratio of 5 ppbv acetone. Under most atmospheric conditions, this interference is negligible. No significant interferences were found for atmospheric concentrations of reactants during ozonolysis experiments. Only for propene, α-pinene, limonene, and isoprene at reactant concentrations, which are orders of magnitude higher than in the atmosphere, could artificial OH be detected. The value of the interference depends on the turnover rate of the ozonolysis reaction. For example, an apparent OH concentration of approximately 1×10^6 cm^{-3} is observed when 5.8 ppbv limonene reacts with 600 ppbv ozone. Experiments with the nitrate radical NO_3 reveal a small interference signal in the OH, HO_2, and RO_2 detection. Dependencies on experimental parameters point to artificial OH formation by surface reactions at the chamber walls or in molecular clusters in the gas expansion. The signal scales with the presence of NO_3 giving equivalent radical concentrations of 1.1×10^5 cm^{-3} OH, 1×10^7 cm^{-3} HO_2, and 1.7×10^7 cm^{-3} RO_2 per 10 pptv NO_3.

Published by Copernicus Publications on behalf of the European Geosciences Union.

1 Introduction

The hydroxyl radical, OH, is the key reactant that controls the chemical transformation of pollutants and their removal in the atmosphere (Finlayson-Pitts and Pitts Jr., 2000). In situ measurements in the field have been used to test our understanding of radical chemistry in the atmosphere.

Model–measurement comparisons of OH concentrations have shown a significant discrepancy for field campaigns in forested areas where concentrations of biogenic volatile organic compounds are large and nitrogen monoxide, NO, concentrations are low (Rohrer et al., 2014). For these conditions the recycling of OH by the reaction of peroxy radicals (RO_2 and HO_2) with NO is inefficient. Recently, other radical reactions such as uni-molecular isomerization and decomposition of RO_2 have been recognized to contribute to the reformation of OH (e.g. Peeters et al., 2014). Despite the progress in the understanding of the OH chemistry in such environments, the unexpectedly high measured OH concentrations are still only partly explained. Therefore, the question whether OH measurements could have been affected by artifacts also needs to be investigated (Fuchs et al., 2012).

Observations of nighttime OH concentrations are larger than predicted by model calculations in a number of field campaigns in forested and urban environments (Lu et al., 2014, and ref. therein). During our field campaigns in China 2006, nighttime OH concentrations reached values up to 3×10^6 cm^{-3}. In the absence of daylight, OH concentrations are expected to be small, because primary OH sources by the photolysis of ozone and nitrous acid are not present. In addition, radical recycling via peroxy radicals is suppressed, because also NO concentrations are small due to the lack of production by the photolysis of nitrogen dioxide (NO_2). However, NO can also accumulate during nighttime, when all ozone has already been titrated. Oxidation of organic compounds is expected to occur predominantly by reactions with ozone and the nitrate radical NO_3. Unknown reactions of these nighttime oxidants with anthropogenic or biogenic VOCs may enhance nocturnal OH concentrations in the atmosphere as discussed by Lu et al. (2014), but may also cause interferences in the instrument.

Laser-induced fluorescence (LIF) is a widely used technique for the direct detection of atmospheric OH radicals. In general, laser-wavelength modulation is applied to distinguish the OH fluorescence from non-resonant, laser-excited background signals. The concept cannot, however, discriminate between fluorescence from ambient OH, which is sampled into a low-pressure cell, and OH that may be artificially produced inside the detection cell. In recent field studies, significant artifacts from spurious OH have been reported for two LIF OH instruments (Mao et al., 2012; Novelli et al., 2014a), when the sampled air contained alkenes and ozone. The artifacts were discovered by applying a chemical titration scheme that destroys ambient OH before entering the low-pressure detection cell. In this operational mode, the remaining OH signal is considered to be an interference from internal OH production that can be used for correction of the ambient OH measurement.

The contribution of artificial OH to the total OH was found to be 30 to 70 % during daytime for measurements in a forest in California (Mao et al., 2012) and up to 80 % during daytime in a boreal forest in Finland (Hens et al., 2014; Novelli et al., 2014a). In these campaigns, OH that was measured during nighttime was often found to be exclusively internally produced. Griffith et al. (2013) estimated that 50 to 100 % of the measured nighttime OH could have been due to internal OH production in a forest site in Michigan, but the experimental set-up for the chemical titration was very preliminary. No significant unexplained internal OH was found in later tests (Griffith et al., 2013).

The reason for the large interferences found in the instruments used in Mao et al. (2012) and Novelli et al. (2014a) is not fully clear, but the authors of both studies hypothesize that internally produced OH could be related to the short-lived products of the ozonolysis of alkenes. In a subsequent laboratory study, stabilized Criegee intermediates (sCIs) that are produced in the ozonolysis reaction were found to decompose to OH in the inlet of one of the instruments (Novelli et al., 2014b). This could be an explanation of the artificial OH that was found in the field for this instrument.

In a previous study (Fuchs et al., 2012), we investigated potential OH interferences in our LIF instrument (Forschungszentrum Jülich) during the photo-oxidation of alkenes (including trans-2-butene and isoprene) and aromatics for similar chemical conditions as found in the field campaigns in the Pearl River Delta and Beijing in China, during which measured OH concentrations were larger than expected (Hofzumahaus et al., 2009; Lu et al., 2012, 2013). The experiments were performed with sunlight in the atmosphere simulation chamber SAPHIR in Jülich. OH concentrations reached values of 1×10^7 cm^{-3} and ozone concentrations were 20 to 50 ppbv. OH concentrations were simultaneously measured by LIF and open-path differential optical absorption spectroscopy (DOAS), which served as an absolute reference. The comparison of the two techniques gave no indication of significant interferences in the OH detection of the LIF instrument during the photo-oxidation of CO, methane, trans-2-butene, isoprene, methacrolein, benzene, p-xylene, and mesitylene. Small interferences from toluene and methyl vinyl ketone, yet far too small to explain the OH concentrations observed in the field campaigns in China, could not be excluded.

Here, we report new experimental results concerning potential interferences in the OH detection for the LIF instruments of Forschungszentrum Jülich that could be particularly relevant at night. Experiments investigated the ozonolysis of various alkenes and the presence of nitrate radicals. In addition, the artificial production of OH by laser photolysis of acetone was tested.

2 Experimental

2.1 RO_x detection by laser-induced fluorescence

The detection of atmospheric OH radicals is accomplished by applying laser-induced fluorescence technique in the Jülich instruments. Details of the instruments that were deployed in previous field and chamber experiments are described in Holland et al. (2003); Fuchs et al. (2008b, 2012); Lu et al. (2012). Here, we used the instrument that is permanently installed at the atmosphere simulation chamber SAPHIR (Fuchs et al., 2012). This instrument is similar to the instruments that were deployed in previous field campaigns on the ground and on board of a Zeppelin (e.g. Lu et al., 2012, 2013; Li et al., 2014). It contains three separate fluorescence cells for the detection of OH, HO_2, and RO_2 radicals. In addition to this instrument, experiments were done with the OH channel of a newly developed instrument that can be deployed on an aircraft (Broch, 2011).

The body of the OH detection cell of the aircraft instrument has the same cubical design and size as the ground-based version. However, it differs in the distance between the tip of the inlet and the fluorescence detection (Fig. 1), which needs to be longer in order to sample ambient air through the aircraft fuselage. In the current work, the OH cell of the aircraft instrument was used to study the possible influence of the extended gas inlet on potential interferences for otherwise comparable experimental conditions used for ground-based measurements. Both ground-based and aircraft measurement cells have a critical inlet nozzle with an orifice diameter of 0.4 mm (1 standard L min^{-1} sampling flow rate) and were operated at the same cell pressure (4 hPa). In both cells, a sheath flow of 1 standard L min^{-1} of dry nitrogen was added downstream of the inlet nozzle. The conically shaped inlet nozzles (both have an opening angle of 70°) differ between the two instruments with respect to their exact shape and the material. The nozzle of the instrument with the short inlet consists of a commercial skimmer (Beam Dynamics) made of thin nickel (orifice edge maximum thickness is 10 µm), which is welded on a stainless steel flange that is mounted on top of the fluorescence cell. The nozzle of the cell with the long inlet is made of anodized aluminium (wall thickness approx. 0.7 mm) with a flat top (diameter 2.5 mm), through which the orifice is drilled. The distance between the tip of the inlet nozzle and the detection by laser-induced fluorescence is minimized for the instrument with the short inlet (approximately 10 cm) but is approximately 32 cm long in the aircraft instrument.

From previous studies with short-inlet measurement cells, we know that the gas expansion through the inlet nozzle produces a fast, collimated gas jet, which has a diameter of about 1 cm when it crosses the detection volume after a travelling time of 1 to 2 ms (Holland et al., 1995; Fuchs et al., 2011). In case of the long inlet, the gas beam eventually slows down, mixes with the sheath gas and fills the whole cross section of the inlet tube. The estimated residence time for air between sampling and detection is on the order of 30 ms. In both cells, baffle arms that are attached to minimize laser stray light are permanently purged with a small flow of nitrogen (flow rate 0.2 L min^{-1}).

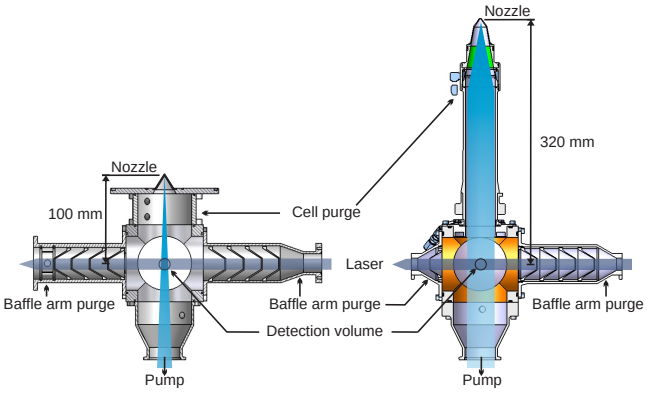

Figure 1. The two cell designs for OH detection by LIF for ground-based measurements (left) and measurements on an aircraft, which requires a longer inlet (right). The estimated residence time for the detection cell with the short inlet is 1.6 ms, much shorter compared to the cell with the long inlet (approximately 30 ms). Windows are placed where the laser enters and exits the fluorescence cells.

In the centre of the fluorescence cell, OH is excited by a short (duration 25 ns), single-path laser pulse at 308 nm at high repetition rate (instrument with the short inlet: 8.5 kHz; instrument with the long inlet: 3 kHz). The fluorescence is detected by a gated multi-channel plate photomultiplier (MCP) with a time delay of approximately 100 ns, in order to protect the MCP against laser stray light. Signals of the MCP are measured by time-resolved single photon counting. In order to distinguish between background and fluorescence signals, the wavelength of the laser is periodically moved from on resonance wavelengths to off resonance wavelengths of the OH absorption line. Because the number of fluorescence photons is proportional to the laser power, all count rates shown in this work are normalized to the laser power that is monitored at the exit of the fluorescence cell by a photodiode.

Hydroperoxy (HO_2) and organic peroxy (RO_2) radicals are detected in separate fluorescence cells via chemical conversion to OH (Fuchs et al., 2008b, 2011).

The HO_2 detection cell is similar to the one for OH, but NO is injected downstream of the inlet nozzle in order to convert HO_2 to OH before the air reaches the laser excitation region of the fluorescence cell. Some specific RO_2 species can be converted to OH on a similar timescale, but this requires two sequential reaction steps with NO (Fuchs et al., 2011). Therefore, interferences from RO_2 in the HO_2 detection can be minimized by choosing an NO concentration, for which the HO_2 conversion efficiency is only approximately 10 %.

The measurement of RO_2 radicals is achieved in a third detection channel applying a two-step conversion of RO_2 to OH (Fuchs et al., 2008b). A conversion reactor upstream of the fluorescence cell is operated at a pressure of 25 hPa and is equipped with an inlet nozzle with 1 mm diameter resulting in a sampling flow rate of 7 standard L min^{-1}. The residence time of sampled air is approximately 0.6 s. Sufficient NO (0.7 ppmv) is added (RO_x mode) in order to convert RO_2 to HO_2 quantitatively. Because HO_2 is converted to OH at the same timescale, radical termination reactions of OH with NO and wall loss would reduce the transmission of radicals through the conversion reactor. Therefore, also excess CO is added, so that OH is reconverted to HO_2, which has smaller wall loss compared to OH through the conversion reactor. As a result, all RO_x species ($OH+HO_2+RO_2$) are converted to HO_2. The conversion reactor can also be operated without addition of NO (HO_x mode), leading to the conversion of $OH+HO_2$ and part of the RO_2 to HO_2. Half of the air in the conversion reactor is sampled into a fluorescence cell downstream of the conversion reactor; the other half is pumped away. This fluorescence cell is similar to the one for HO_2 detection, but the inlet nozzle and the amount of NO that is injected are different. Because the pressure in the conversion reactor is already reduced, the orifice of the inlet nozzle has a diameter of 4 mm and the NO concentration is chosen to maximize the conversion efficiency of HO_2 to OH.

The limit of detection ($1\,\sigma$) of the OH measurement is 0.3×10^6 cm^{-3} for both instruments with the short and long inlet and 1.5×10^7 cm^{-3} for HO_2 and RO_2 at a time resolution of 47 s. The 1σ accuracy of the radical detection is limited by the accuracy of the calibration to 10 % for all instruments and radical species. The accuracy is lowered in experiments with high ozone concentrations because a significant background signal due to the presence of ozone needs to be subtracted.

2.2 OH detection by DOAS

DOAS is a calibration-free method to measure OH concentrations. Only one instrument currently exists for atmospheric OH detection, which is installed in the atmosphere simulation chamber SAPHIR in Jülich. Details of the instrument can be found elsewhere (Hausmann et al., 1997; Schlosser et al., 2007, 2009).

Broad-band UV radiation at 308.04 nm is produced by a frequency-doubled picosecond dye laser that is synchronously pumped by a picosecond, passively mode-locked, diode-pumped Nd:YAG laser with internal frequency doubling to 532 nm. The laser beam is coupled into an optical multiple reflection cell (modified White cell type), whose mirrors have a distance of 20 m along the centre of the cylindrically shaped chamber (total absorption path length: 2240 m). The absorption signal is detected by a high-resolution echelle spectrometer. The limit of detection for the OH measurement by this DOAS instrument is 8×10^5 cm^{-3} at a time resolution of 3 min. The 1σ accuracy is 7 %.

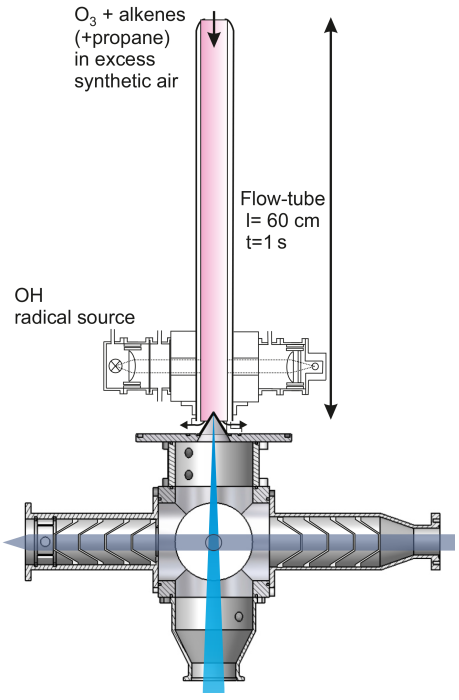

Figure 2. Set-up for laboratory ozonolysis experiments. Reactants are flowed through a 60 cm long flow tube (OH radical source) mounted on top of the fluorescence cell (scales of the radical source differs from the scale of fluorescence cell). The cell with the short inlet is shown, but the set-up was the same for the cell with the long inlet.

2.3 Laboratory experiments

2.3.1 Ozonolysis experiments

Laboratory experiments made use of a flow tube that was mounted on top of the fluorescence cell in order to over flow the inlet with a mixture of synthetic air of highest purity (purity 99.99990 %; Linde) with various reactants. For this purpose, the radical calibration source described in Fuchs et al. (2011) was used (Fig. 2). Essentially, a 60 cm long glass tube (inner diameter 1.9 cm) was mounted upstream of the inlet. The residence time of air was approximately 1 s at a flow rate of 10 L min^{-1} used in most of the experiments shown here. When not stated otherwise, all experiments were performed in dry synthetic air. Humidification was achieved by passing the gas through a water bubbler containing Milli-Q water.

In addition, the radical source can provide OH by water vapour photolysis at 185 nm in order to calibrate the instrument sensitivity. In this case, radiation of a mercury lamp illuminated humidified synthetic air in a short distance to the tip of the inlet nozzle (approximately 6 cm). The time between OH production and sampling was only approximately

30 ms at a typical flow rate of 20 L min^{-1} for calibration purposes.

For ozonolysis experiments, reactants were mixed at the inlet of the glass tube. Ozone was produced by a home-built ozone generator making use of oxygen photolysis by the 185 nm radiation of a mercury lamp with subsequent reaction of the oxygen atom with an oxygen molecule. A small flow of either oxygen or synthetic air was flowed through a quartz glass tube at a flow rate of maximum 200 mL min^{-1} and mixed into the large flow of synthetic air. Ozone concentrations were varied by changing the flow rate or the current of the mercury lamp. Ozone mixing ratios were as high as 1 ppmv and were measured by UV photometry (Ansyco).

Organic compounds were either provided from gas bottles (purities: propane and propene 99.95 %, 1-butene 99.5 %; Linde) or from liquids (purities: limonene, isoprene, 2,3-dimethyl-2-butene > 99 %, α-pinene 98 %; Sigma-Aldrich). In both cases, mixtures of organic compounds in nitrogen with appropriate mixing ratios were prepared in small Silcosteel canisters. Liquid compounds were injected into the canister and diluted with nitrogen. Mixing ratios were chosen, such that a small flow of maximum 100 sccm could be mixed into the large flow of synthetic air in order to provide the desired mixing ratios of reactants. SO_2 and CO were taken from gas mixtures in nitrogen (purities: SO_2 99.98 %, CO 99.997 %; Linde).

2.3.2 Experiments with NO_3 and N_2O_5

For tests with NO_3 and N_2O_5, a Teflon tube that contained an injection needle to inject NO_3 and N_2O_5 was mounted between the flow tube and the measurement cell (Fig. 3). This Teflon tube was 10 cm long and had an inner diameter of 1.7 cm. The residence time of air was approximately 10 ms at a flow rate of 10 L min^{-1} of synthetic air that was provided by the radical source that was mounted on top of the Teflon tube.

In order to provide NO_3 and N_2O_5, a similar set-up was used as applied for the characterization of a cavity ring-down instrument for NO_3 detection (Fuchs et al., 2008a). N_2O_5 was produced in a two-step synthesis in two subsequent flow tubes made of glass. In the first tube, NO (purity: 99.5 %; Linde) quantitatively reacted with excess oxygen (purity: 99.999 %; Linde) to NO_2. In the second glass tube, ozone produced by a silent discharge ozone generator was added, so that part of the NO_2 was oxidized to NO_3. In a subsequent reaction of NO_3 with NO_2 the N_2O_5 was formed. It was captured in crystalline form in a dry ice cold trap.

A small flow (maximum flow rate 100 mL min^{-1}) of nitrogen was flowed over the frozen N_2O_5 to use the system as an NO_3/N_2O_5 source. The air that had passed the N_2O_5 could be guided through a heated tube at 120 °C, so that N_2O_5 thermally decomposed to NO_3 and NO_2. A mixture of NO_3 and N_2O_5 was always present, since NO_3 and N_2O_5 started to thermally equilibrate at room temperature. The residence time in the tubing system that was not actively heated or cooled, however, was short, so that the majority was either NO_3 (with heater) or N_2O_5 (without heater). The small air flow from the N_2O_5/NO_3 source was then mixed into the large flow of synthetic air via an injection needle at the entrance of the Teflon tube.

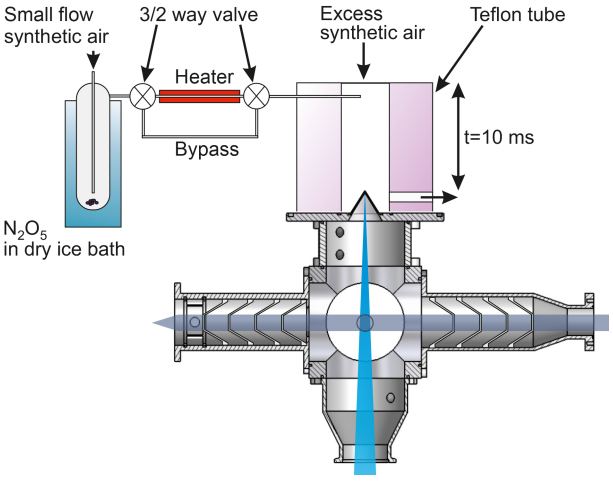

Figure 3. Set-up for laboratory experiments testing NO_3/N_2O_5. Frozen N_2O_5 is over flowed by nitrogen. The source can be switched to an NO_3 source if N_2O_5 is thermally decomposed in a heater. This flow is injected into a large flow of synthetic air provided by the radical source that is mounted on top of the Teflon tube (not shown here, see Fig. 2). Only a small part is sampled by the instrument. The cell with the short inlet is shown, but the set-up was the same for the cell with the long inlet.

N_2O_5 and NO_3 concentrations depended on the flow rate of nitrogen through the trap but were not quantified here. Tests with a cavity ring-down instrument that is capable of measuring NO_3 concentrations have shown that mixing ratios of several ppbvs can be achieved in a similar set-up (Fuchs et al., 2008a). The exact concentration, however, was not exactly reproducible for several reasons: instability of the N_2O_5 source, surface losses, and a not well-defined mixing efficiency of the large flow of synthetic air and the small flow containing NO_3/N_2O_5.

2.4 Experiments in the simulation chamber SAPHIR

Additional experiments were performed in the simulation chamber SAPHIR. These experiments allowed the comparison of OH measurements by the LIF instrument with other measurements, e.g. those by the DOAS instrument. SAPHIR can be regarded as a large chemical reactor that provides a homogeneous mixture of trace gases in synthetic air, ensuring that instruments sampled the same air mass. It has been shown in several comparison exercises that this assumption is justified for OH (Schlosser et al., 2007, 2009; Fuchs et al., 2012). Details of the chamber can be also found in these publications.

SAPHIR is a cylindrically shaped (length 18 m, diameter 5 m) outdoor chamber. It consists of a double-wall Teflon film. The chamber is equipped with a shutter system that was closed at all times during experiments here. Synthetic air was provided from evaporated liquid nitrogen and oxygen (purity 99.99990 %; Linde). The chamber was operated at slightly higher pressure than ambient pressure to prevent leakages into the chamber. Air that had been lost by leakages and air consumption by instruments was continuously replaced by a replenishment flow.

The chamber was flushed with synthetic air before each experiment, until all trace gas concentrations were below the limit of detection of instruments. No significant sources of trace gases were observed in the clean, dark chamber. For experiments here, NO_2 was detected by a chemiluminescence instrument, O_3 by UV photometry and organic compounds by proton-transfer-reaction mass spectrometry. Furthermore, the DOAS instrument (see above) served as reference instrument for OH. During one experiment, NO_3 concentrations were quantified by a home-built cavity ring-down instrument similar to the instruments described in Fuchs et al. (2009) and Wagner et al. (2011).

The chamber air was humidified in one experiment by boiling water from a Milli-Q device. The water vapour was flushed into the chamber by a large flow of synthetic air. NO_2 was injected from a mixture of NO_2 (purity: 99 %; Linde) in nitrogen by a mass flow controller. Ozone was produced by a silent discharge ozonizer and organic compounds (purities: α-pinene 98 %, acetone 99.8 %; Sigma-Aldrich) were injected as liquids in a heated inlet and then purged into the chamber by the replenishment flow of the chamber.

3 Tests for interference from the photolysis of acetone

Blitz et al. (2004) reported that the photo-dissociation of acetone (CH_3COCH_3) below 338 nm yields acetyl (CH_3CO) radicals with a large quantum yield at low pressure.

$$CH_3COCH_3 + h\nu(308\,\text{nm}) \rightarrow CH_3CO + CH_3 \quad \text{(R1)}$$

$$CH_3CO + O_2 \rightarrow OH + \text{products} \quad \text{(R2)}$$

$$CH_3CO + O_2 + M \rightarrow CH_3CO(O_2) + M \quad \text{(R3)}$$

The acetyl radicals can react with oxygen and form acetylperoxy radicals in a pressure-dependent reaction (Reaction R3) or they can produce OH in a bimolecular reaction (Reaction R2). At low pressure, the OH production dominates. Thus, acetone photolysis can lead to internal OH production in the low-pressure cell of the OH LIF instrument.

In order to test for this interference, an experiment in the dark SAPHIR chamber was performed during which a large amount of acetone was injected. This test was done with the instrument with the short inlet and the high laser repetition rate. Calculations using the amount of acetone that was injected yield a mixing ratio of 950 ppbv acetone after injection. Acetone was then purged out of the chamber by the replenishment flow of the chamber. An artificial OH signal was observed in the OH LIF instrument. This signal that is already normalized to laser power depends linearly on laser power as expected from a photolytic process that is caused by the 308 nm radiation. The interference signal was equivalent to 0.05×10^6 cm^{-3} OH for a mixing ratio of 5 ppbv acetone at a typical laser power of 10 mW. The value of this acetone interference is very similar to the one that was reported for another LIF OH instrument using 308 nm laser excitation (Ren et al., 2004).

Acetone mixing ratios in the atmosphere are often only a few ppbv (Monks et al., 2009, and ref. therein) but can reach up to 10 ppbv close to anthropogenic sources (Yuan et al., 2015). Therefore, the interference due to acetone photolysis at 308 nm can be assumed to be well below the limit of detection of the instrument in most cases. Nevertheless, this interference has the potential to become significant for higher laser power than used here and/or exceptionally large acetone concentrations.

4 Test for interferences from products of the ozonolysis of alkenes

4.1 Results of laboratory ozonolysis experiments

OH radicals and organic compounds are expected to be produced in the reaction of ozone with alkenes (e.g. Atkinson et al., 2006). If a sufficient concentration of a chemical OH scavenger is added, OH concentrations can be suppressed. If OH is also detected in the presence of the scavenger, internal OH production inside the instrument is indicated.

A first series of experiments investigated the ozonolysis of 1-butene, 2,3-dimethyl-2-butene, α-pinene, limonene, and isoprene for both cell configurations. Details of the experimental conditions for tests are shown in Table 1 and results in Fig. 4.

In the first step of the experimental procedure, only ozone was added to the synthetic air in the flow tube (Fig. 2). Ozone itself can cause a small interference signal inside the measurement cell (Holland et al., 2003). Therefore, the OH signal without the addition of organic compounds but with ozone was always measured separately in each experiment and subtracted from the signal obtained in the presence of the alkene and ozone. The exact value varied among experiments. The reproducibility of the ozone background measurement limited the accuracy of OH in these experiments. Therefore, also the limit of detection of approximately 1.5×10^6 cm^{-3} was higher compared to field measurements, when ozone concentrations are much lower. Maximum values of this interference signal were a few counts per second equivalent to an OH concentration of a few 10^6 cm^{-3} for experiments with hundreds of ppbv ozone. These values were similar in experiments with both instruments.

Table 1. Experimental conditions during flow tube ozonolysis experiments in dry synthetic air shown in Figs. 4 and 5. Laser power was around 13 mW.

	Alkene/ ppbv	O_3/ ppbv	Turnover rate ozonolysis[a]/ ppbv h^{-1}	Propane/ ppmv	OH signal without propane/ 10^6 cm^{-3}	OH signal with max. propane/ 10^6 cm^{-3}
TME[b,c]	0.2	390	8	0 to 10	29	< LOD[d]
1-Butene[c]	2.5	900	2	0 to 10	2.2	< LOD[d]
α-Pinene[c]	2.3	600	11	0 to 10	11	< LOD[d]
Limonene[c]	0.5	390	4	0 to 10	6.3	< LOD[d]
Isoprene[c]	7.3	900	7	0 to 10	2.6	< LOD[d]
TME[b,e]	0.6	40	2.3	0 to 10	12	< LOD[d]
1-Butene[e]	19	800	11.5	0 to 10	3	< LOD[d]
α-Pinene[e]	4.6	700	25	0 to 10	12	< LOD[d]
Limonene[e]	0.9	800	13	0 to 10	11	< LOD[d]
Ethene[c]	2400 to 12 000	800	1270[g]	100	[f]	< LOD[d]
Propene[c]	200 to 1700	300	500[g]	100	[f]	4.6[g]
α-Pinene[c]	1 to 70	600	320[g]	60	[f]	4.6[g]
Limonene[c]	1 to 70	600	820[g]	200	[f]	14[g]
Limonene[c]	30	0 to 650	300[h]	180	[f]	7.5[h]
Isoprene[c]	1 to 450	900	450[g]	20	[f]	6.4[g]

[a] Room temperature, ambient pressure
[b] 2,3-Dimethyl-2-butene
[c] Instrument with long inlet
[d] Increased limit of detection (LOD) due to the subtraction of the ozone background
[e] Instrument with short inlet
[f] Not quantified
[g] For maximum alkene conc. tested
[h] For maximum ozone conc. tested

In the next step, an alkene was added to the air that contained ozone. Concentrations of ozone and organic compounds were chosen, such that a significant OH signal could be measured. OH production in the flow tube is expected from the decomposition of products formed in the ozonolysis reactions (e.g. Atkinson et al., 2006). After having adjusted the concentration of reactants, various amounts of propane were added at the entrance of the flow tube in order to scavenge OH that is produced in the flow tube. Propane mixing ratios were increased to up to 10 ppmv. In this case, the lifetime of OH in the flow tube is 4 ms, much shorter than the residence time of air (1 s).

The sufficient titration efficiency is demonstrated by the complete removal of OH that is produced by the calibration source (Fig. 4), when OH is produced by water photolysis. The reaction time is only approximately 30 ms in this case, because OH is produced close to the inlet nozzle of the fluorescence cell.

In contrast, the lifetime of OH inside the measurement cell is increased by a factor of approximately 250 due to the reduced pressure (e.g. 1 s in the presence of 10 ppmv propane). This is much longer than the residence time of the sampled air (1.6 and 30 ms for the two cell configurations) before excitation by the 308 nm radiation. Therefore, internally produced OH does not significantly react with propane. An example for internal OH production is given by the ozone interference signal, which is constant for all propane mixing ratios tested (up to 100 ppmv, only shown up to 10 ppmv in Fig. 4).

For OH signals obtained during ozonolysis reactions shown in Fig. 4, contributions from ozone alone are already subtracted and concentrations are normalized to the OH concentration that was present in the absence of propane. The measured OH concentration drops with increasing propane concentration until the OH signal is below the limit of detection. This indicates that no detectable internal OH production is observed for the ozonolysis reactions tested here.

Further experiments were conducted at much higher concentrations of ethene (with mixing ratios up to 12 ppmv, propene (with mixing ratios up to 1.7 ppmv) and limonene, α-pinene (both with mixing ratios up to 70 ppbv), and isoprene (mixing ratios up to 450 ppbv) and ozone mixing ratios of up to 900 ppbv using the cell with the long inlet (Table 1). Sufficient propane was always added to scavenge externally produced OH during these experiments.

Significant internal OH production is observed in the case of high propene, α-pinene, limonene, and isoprene concentrations (Table 1). In the case of ethene, no significant signal is observed. The laser excitation spectrum demonstrates that the signal originates from OH. Because OH produced in the

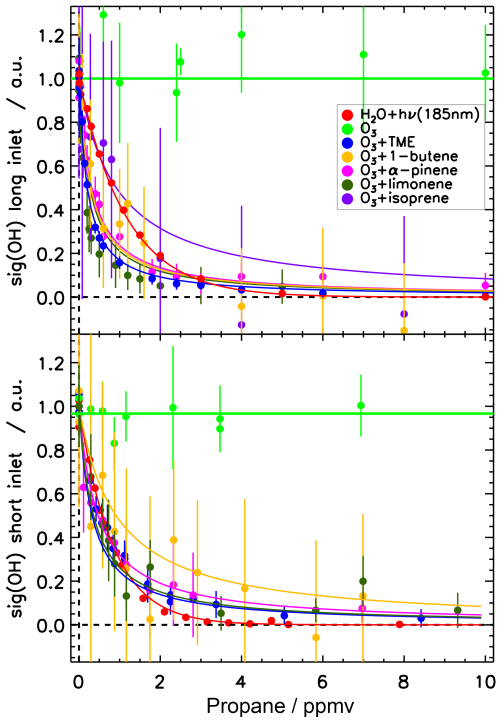

Figure 4. Relative OH signals during flow tube experiments depending on the propane mixing ratio. Each decay curve (distinguished by different colours) corresponds to a different OH production mechanism. OH was produced by water photolysis (normal operation of the calibration source), by ozone inside the cell, or by ozonolysis of various alkenes in dry air. Lines are arbitrary fits to guide the eye in this plot. Results obtained with the cell with the long inlet (top) and short inlet (bottom) are shown here. Experimental conditions can be found in Table 1.

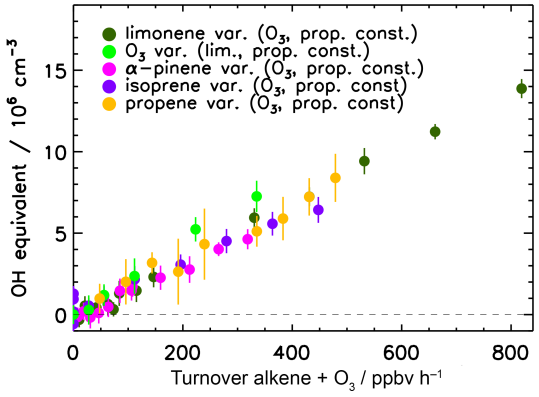

Figure 5. Signals as OH equivalents during flow tube experiments using the cell with the long inlet for very high alkene and ozone concentrations in the presence of high concentrations of propane as OH scavenger. Experimental conditions are shown in Table 1. An unexplained OH signal is observed, which correlates with the turnover rate of the alkene ozonolysis reaction (room temperature and ambient pressure). Turnover rates are not high enough to explain observed OH production inside the fluorescence cell due to the dilution of reactants at the reduced pressure of 4 hPa.

flow tube is titrated by propane, OH is apparently caused by internal production. Except for ethene, the signal scales linearly with both the alkene and the O_3 concentration. Figure 5 shows this interference signal as equivalent OH concentrations depending on the turnover rate of the ozonolysis reaction at room temperature and ambient pressure, which was calculated as the product of the alkene and ozone concentrations and the reaction rate constant of the ozonolysis reaction. Similar slopes of this relationship are obtained when either the concentration of any of the four species were varied at constant ozone concentration or when the ozone concentration was changed in the presence of a constant limonene concentration. According to the dependencies in Fig. 5, an interference with an apparent OH concentration of 1×10^6 cm^{-3} is obtained in the presence of 100 ppbv ozone and 65 ppbv α-pinene or 30 ppbv limonene, 480 ppbv isoprene, or 600 ppbv propene.

Several tests were conducted in order to characterize the interference signal (Fig. 6). It does not depend on the power of the 308 nm laser and did not change in the presence of water vapour (up to a mixing ratio of 1.2 %), when 1 ppmv α-pinene reacted with 110 ppbv ozone. SO_2 (up to a mixing ratio of 4 ppmv) was added, when 40 ppbv limonene reacted with 550 ppbv ozone in the presence of 400 ppmv propane, but the interference signal stayed nearly constant. Signals became only noisier in the presence of SO_2 because of an increased background signal due to SO_2 fluorescence at 308 nm.

However, the interference signal depends on the pressure inside the fluorescence cell. During these test experiments, 45 ppbv limonene and 350 ppbv ozone were added. Here, changes of the OH detection sensitivity need to be taken into account and therefore signals were normalized by the measured OH detection sensitivity to be comparable. For both cell configurations, the signals become smaller with decreasing cell pressure. The magnitude of the signal, however, is larger for the cell with the long inlet compared to the one with the shorter inlet.

4.2 Results of ozonolysis experiments in the SAPHIR chamber

In order to test potential interferences from alkene ozonolysis products for a longer timescale than in the flow tube and with concurrent measurements by the OH reference instrument DOAS, two experiments were performed in the atmosphere simulation chamber SAPHIR.

Experiments started with clean, dry synthetic air. During the experiments, ozone and α-pinene were injected into the chamber several times (Fig. 7). First, approximately 5 ppbv α-pinene was added together with 140 ppbv ozone. α-pinene reacted away within 2 h. OH measurements by DOAS and LIF instruments (short inlet) agreed within their measure-

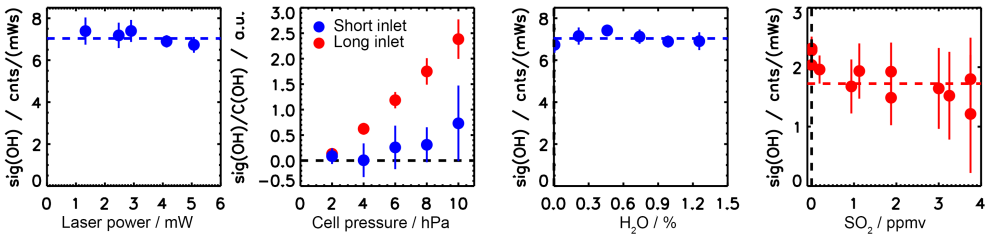

Figure 6. OH signals from limonene or α-pinene ozonolysis depending on various parameters: laser power (1 ppmv α-pinene, 110 ppbv O_3, cell with short inlet), cell pressure (45 ppbv limonene, 350 ppbv O_3, 1000 ppmv propane), water vapour (1 ppmv α-pinene, 110 ppbv O_3, cell with short inlet), and SO_2 (40 ppbv limonene, 550 ppbv O_3, 400 ppmv propane, cell with long inlet). No propane was added for testing the laser power and water vapour dependencies. In these two cases, the concentration of α-pinene was chosen to be high enough, such that the OH signal was dominated by internally produced OH in the detection cell.

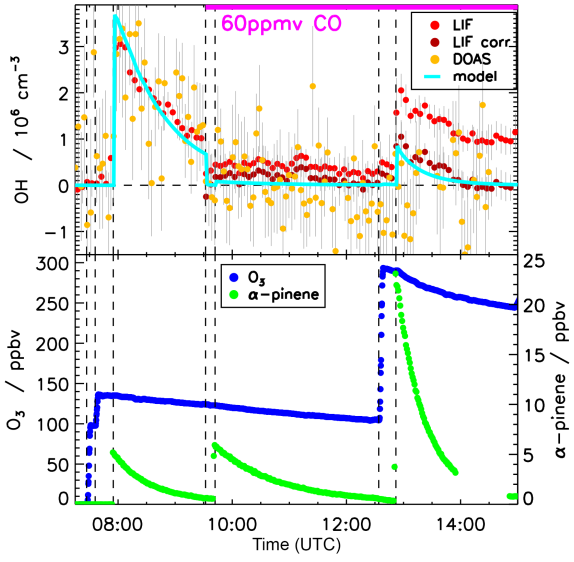

Figure 7. OH measured by LIF (cell with short inlet) and DOAS during the ozonolysis of α-pinene in dry air in the SAPHIR chamber with and without the presence of sufficient CO to scavenge OH. Subtraction of an offset in OH by LIF for each α-pinene oxidation period that would be an interference leads to corrected LIF data (LIF-corr) in reasonable agreement with DOAS and modelled concentrations.

ment errors during this part of the experiment and showed maximum concentrations of 3.5×10^6 cm^{-3}. Also, box model calculations applying MCM (2014) 3.2 (MCM, 2014) reproduce measured OH concentrations if the model is constrained to measured α-pinene and O_3 concentrations and measured temperature and pressure.

Two hours after the first injections of O_3 and α-pinene, 60 ppmv CO was added to scavenge OH produced by the ozonolysis reaction. From that point in time, OH measurements by DOAS scattered around 0. Also, OH concentrations measured by LIF dropped right after the addition of CO, but measured OH concentrations were larger than 0 with 0.3×10^6 cm^{-3}. After a second addition of 5 ppbv α-pinene, OH measured by LIF increased to 0.5×10^6 cm^{-3} and stayed nearly constant until the third α-pinene injection (23 ppbv). Measured OH concentrations then reached a maximum of 2×10^6 cm^{-3} and decreased at later times to 1×10^6 cm^{-3}. This decrease is well correlated with the decrease in the α-pinene concentration. In addition, model calculations show that OH from ozonolysis contributed to the measured OH even in the presence of the OH scavenger, but were too small to be detected by the DOAS instrument. However, like after the second α-pinene a residual OH signal is observed, which is present right after the injection and stays approximately constant over time.

A similar behaviour was observed during the second experiment on the following day, when the experiment was conducted in a similar manner but with humidified air. The unexplained part of the OH signal correlates with the total α-pinene concentration that was added during each experiment (Fig. 8). Residual signals were larger on the second day in the presence of water vapour.

4.3 Discussion

Experiments with low reactant concentrations show that the OH concentration approaches 0 within the uncertainty of measurements with increasing propane concentrations for all species tested here (Fig. 4). These results indicate that no detectable OH is produced inside the fluorescence cell for conditions of these laboratory experiments.

In contrast, a significant, unexpected OH signal is seen in the ozonolysis experiments with very high reactant concentrations of propene, α-pinene, limonene, and isoprene. As shown in Fig. 5 the internal OH production observed from these species depends on the turnover rate of the ozonolysis reaction. Turnover rates in the experiments with low reactant concentrations (Fig. 4) are only within the range of a few ppbv h^{-1}, whereas significant internal OH production is only observed for turnover rates of tens of ppbv h^{-1}. Also experiments in the SAPHIR chamber were performed at high reactant concentrations.

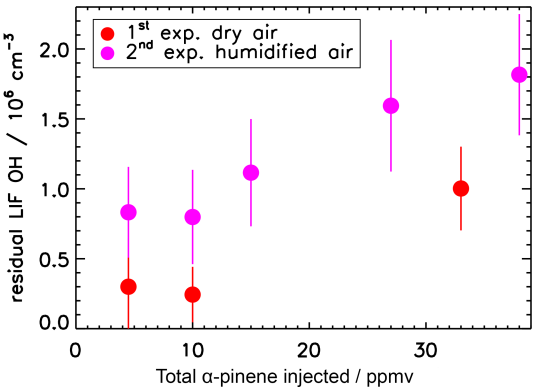

Figure 8. Residual OH signal by LIF (cell with short inlet) for each α-pinene oxidation period during two ozonolysis experiments in the SAPHIR chamber in the presence of CO as OH scavenger depending on the total α-pinene that had been injected during one experiment. One experiment was conducted in dry air (first day) and the other in humidified air (second day). The chamber was flushed with a high flow of synthetic air overnight between the two experiments. Residual concentrations are averaged measurements over 20 min before the next α-pinene injection, when most of the α-pinene had been reacted away.

Reactant concentrations, for which internal OH production is observed, are much larger than typical concentrations in the atmosphere. For example, maximum turnover rates of ozonolysis reactions of monoterpenes were found to be 1.5 ppbv h^{-1} in a boreal forest (Hakola et al., 2012), in which high atmospheric concentrations of monoterpenes are expected. For these atmospheric turnover rates, our experiments demonstrate that no significant internal OH production is expected.

The pressure dependence of the signal that is observed in experiments with high concentrations of monoterpenes and the differences between results obtained with the cell with the long and the short inlet indicate that the internally produced OH depends on the residence time of air in the detection cell and presumably on the exact flow conditions, both of which change with pressure. With increasing pressure, the residence time in the detection cell increases, whereas the loss rate of OH by diffusion to the walls decreases inversely with the pressure. Both effects would be consistent with an increase of OH, which is produced in the gas phase inside the detection cell. The smaller internal OH signal in the cell with the short inlet (shorter residence time of air) gives further support for the conclusion that the internal OH production depends on the residence time in the measurement system. In the following, we discuss which reaction mechanisms could lead to the observed level of internal OH production.

Open questions about the exact reaction mechanism of the ozonolysis of alkenes still exist, especially for alkenes with a high carbon number (Donahue et al., 2011). Ozone adds to the double bond of the organic compound, forming a primary ozonide, which quickly decomposes to a carbonyl oxide (CI) and a carbonyl compound. Gas phase ozonolysis is extremely exothermic, so that the products carry excess energy. The short-lived excited CI can then either decompose or can be stabilized by collisions forming a sCI. Decomposition of the excited CI leads to the formation of OH when the CI is disubstituted or has a syntype structure (Johnson and Marston, 2008).

Direct OH production from the ozonolysis inside the fluorescence cell is too slow to explain the observed internal OH production. Using the slope of the relationship shown in Fig. 5, a reaction time of approximately 140 s would be required to produce the measured OH concentration, much longer than the residence time of air in the fluorescence cell. Furthermore, photolysis reactions by the 308 nm laser can be excluded, because the interference signal is independent of the laser power. For the same reason OH production by the reaction of the alkene with $O(^1D)$ produced by ozone photolysis can be excluded as an explanation.

Another possibility is the formation of a longer-lived product from the ozonolysis, which accumulates in the flow tube and then decomposes to OH in the measurement cell. For the given experimental conditions (Table 1), product molecules with a concentration on the order of 10^9 to 10^{10} cm^{-3} are produced within the residence time of 1 s. After transfer into the measurement cell, conversion of a small fraction (0.1 to 1 %) of these molecules to OH would be sufficient to explain the observed internal OH signals. The conversion efficiency would be compatible, for example, with a uni-molecular decay process with a rate coefficient on the order of 0.2 s^{-1} given a residence time of 30 ms and an OH wall-loss rate coefficient of 65 s^{-1} (Broch, 2011) in the measurement cell. A faster uni-molecular decay (up to about 30 s^{-1}) would still be consistent with the observed internal OH signal. A higher decay rate increases the efficiency of OH production in the detection cell but would deplete more efficiently the hypothetical OH precursor in the flow tube, thereby limiting the amount of internally produced OH.

Stabilized CIs formed in the ozonolysis reaction have the potential to decompose in the inlet of LIF instruments for OH detection, as shown by Novelli et al. (2014b). The sCI yield for molecules which give internal OH production has been determined to be 15 % for α-pinene, 27 % for limonene, and 58 % for isoprene (Sipilä et al., 2014; Donahue et al., 2011; Newland et al., 2015b). The chemistry of the sCI is diverse and is subject to recent research that has been summarized in recent reviews (Taatjes et al., 2014; Lee, 2015). The sCI can decompose and form OH like the excited CI, but its lifetime is often long enough that it can also react with other molecules, for example SO_2 or water vapour (Mauldin III et al., 2012; Vereecken et al., 2012, 2014). The decomposition rate of the sCI is not well known. Published data lie in the range between 3 s^{-1} (Novelli et al., 2014b) and 288 ± 275 s^{-1} (Newland et al., 2015a) for CH_3CHOO in

the syn-conformation that is produced in the ozonolysis of propene and (E)-2-butene.

Because OH and sCIs are both formed by the decomposition of the excited Criegee intermediate, it is expected that sCIs are present during the laboratory ozonolysis experiments at low and high reactant concentrations (Figs. 4 and 5). Although the yield of sCIs is often less than 50 %, even larger concentrations compared to OH that is simultaneously produced in the ozonolysis reactions can be assumed here. Because there are no reaction partners for the sCI in these experiments, the lifetime of the sCI is most likely much longer than that of OH that can also react with the alkene that is present. Consequently, sCIs are presumably present in the flow tube for conditions when OH could be observed from the ozonolysis reaction (in the absence of an OH scavenger) also in the experiments when no internal OH production is observed.

In the case of ethene, the Criegee intermediate CH_2OO is formed, which is not expected to efficiently produce OH (Johnson and Marston, 2008). In the case of propene, however, the stabilized Criegee CH_3CHOO is formed. Novelli et al. (2014b) showed that CH_3CHOO can decompose in the inlet of an LIF instrument for OH detection. In that work, the reaction of 500 ppbv ozone with 70 ppmv propene gave apparent OH concentrations of up to 1×10^8 cm^{-3} in the presence of propane as OH scavenger. The authors also show that the efficiency of the detection has a maximum at a few milliseconds after the air has entered the detection cell. Scaling results at this high turnover rate of the ozonolysis reaction to the turnover rates used in our experiments gives lower OH concentrations than observed in our experiments. However, no exact agreement is expected because internal OH was partly scavenged by the high propene concentration used in Novelli et al. (2014b).

Sipilä et al. (2014) investigated the reaction of sCIs formed in the ozonolysis of limonene and α-pinene, for which internal OH production is observed in the Jülich LIF instrument. The authors investigated the reaction of sCI with SO_2 for different water vapour mixing ratios by measuring the H_2SO_4 yield. They could show that SO_2 efficiently reacts with sCI formed in the ozonolysis of these two monoterpenes. In addition, they concluded that it is not necessary to distinguish between structurally different sCIs to describe their observations. The authors did not find a significant effect of the H_2SO_4 yield on water, suggesting that the reaction rate constant of the sCI with water is negligibly small compared to the decomposition rate of the sCI consistent with an earlier study (Aschmann et al., 2002). This would be also in agreement with our observations if sCIs were causing the internal OH in our experiments (Fig. 6).

Sipilä et al. (2014) also measured the ratio between the rate coefficient for the sCI loss and the rate coefficient for the reaction with SO_2 to be 2×10^{12} cm^{-3}. In order to estimate an upper limit for the absolute reaction rate constant, we take a lower limit of 3 s^{-1} for the sCI loss by their uni-molecular decomposition, although this value was determined for a different sCI (Novelli et al., 2014b). In this case, the reaction of the sCI with SO_2 at the highest SO_2 mixing ratio tested here (3.8 ppmv) would result in a sCI lifetime of only 1.7 ms in the flow tube. This suggests that sCI would have been significantly reduced by the reaction of SO_2 before entering the fluorescence cell. If sCI decomposition from sCIs that were tested by Sipilä et al. (2014) was the cause for the observed internal OH production, a reduction would have been expected with increasing SO_2 concentration but is not observed (Fig. 6). This result, however, does not rule out that decomposition of sCI species that do not react with SO_2 are the cause of the interference.

Other hypothetical mechanisms to produce OH in the detection cell would be heterogeneous reactions at walls or reactions in molecular clusters formed in the cold gas-expansion.

The residual OH signal, which is observed during the experiments in the chamber, correlates not with the time series of α-pinene but with the total amount of α-pinene that had been injected. In addition, measurements indicate that it is present right after the point in time of the injection. The magnitude of this interference signal is similar to the signal observed during laboratory experiments in dry air with high reactant concentrations (Fig. 5), but experiments here do not allow us to conclude whether the mechanism behind is the same.

One explanation could be internal OH production from an impurity of the liquid α-pinene that would not react with ozone and would therefore persist after the injection of α-pinene. However, neither an impurity nor a mechanism is known that would cause the internal OH production. Also, potential interferences from short-lived and long-lived products of the α-pinene ozonolysis reaction do not fit the observations. The time series of short-lived products are expected to follow the time series of α-pinene, so that internal production from these species are expected to decrease with time after each injection of α-pinene. Longer-lived products accumulate over time and reach maximum concentrations at later times. The higher signal during the second day in the presence of water vapour could hint to the involvement of water vapour, which would be in contrast to observations in the laboratory and therefore hint at a different mechanism.

5 Test of interferences from the nitrate radical

5.1 Laboratory experiments with NO_3

Further laboratory experiments were conducted in order to test whether NO_3 can cause interferences in the Jülich LIF instruments. Figure 9 shows the signal measured in the OH cell of the LIF instruments, when dry synthetic air containing NO_3 is provided. The NO_3 concentration was varied by changing the flow rate through the trap containing frozen

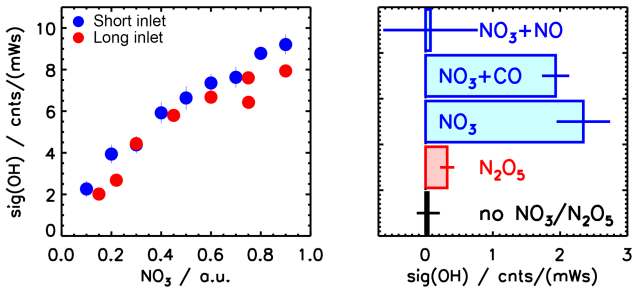

Figure 9. OH signals when air containing NO_3 produced from thermal decomposition of frozen N_2O_5 is sampled for two designs of the OH fluorescence cell. Left panel: variation of NO_3 concentration by changing the air flow through the N_2O_5 source. Right panel: no OH signal (cell with the short inlet) is seen without flow from the N_2O_5 source; only a small signal is observed when N_2O_5 is not actively heated downstream of the source (small efficiency of N_2O_5 dissociation); the large signal is observed when N_2O_5 is sampled through an heated inlet (high efficiency of N_2O_5 dissociation). The signal remains when CO is added to scavenge OH, but disappears when NO is added to scavenge NO_3.

N_2O_5. An OH signal is observed, which correlates with NO_3. The scatter in the data and the small difference in the measurements of the OH cells with the long and the short inlet are most likely caused by changes in the NO_3 concentration due to the instability of the NO_3 source. Excitation spectra show the signature of OH demonstrating that the detected signal stems from OH.

No OH signal is observed if the flow through the N_2O_5 trap is turned off (Fig. 9). If N_2O_5 is quantitatively thermally decomposed to NO_3, a large signal is observed, but this signal becomes small if the air from the trap bypasses the heater. In the latter case, only a small fraction of N_2O_5 thermally decomposes to NO_3 prior sampling. The signal stays nearly constant if a high amount of an OH scavenger is added (0.1 % CO). The small decrease that is observed if this high CO concentration is added could be due to scavenging a small fraction of the internally produced OH. In contrast, the signal drops to 0 if NO is added as a scavenger at the entrance of the flow tube, in order to remove all NO_3, before it enters the measurement cell.

Further laboratory experiments done with the instrument with the short inlet show that the interference signal caused by NO_3 does not depend on laser power of the OH excitation laser, cell pressure, or water vapour (Fig. 10).

5.2 NO_3 experiments in the SAPHIR chamber

In addition to the laboratory experiments, two experiments in the dark SAPHIR chamber were performed, during which NO_3 was produced from the reaction of ozone and NO_2. Fig. 11 shows the time series of O_3 and NO_2. The experiments started in clean, dry synthetic air. O_3 mixing ratios were increased to 140 ppbv and NO_2 was injected two times, reaching maximum mixing ratios of 40 ppbv. NO_3 mixing ratios, which were measured by a newly built CRDS instrument during one of the experiments, exhibited a maximum of 1 ppbv 1 to 2 h after each NO_2 injection.

No OH, HO_2, or RO_2 was expected to be present, because the synthetic chamber air was free from VOCs which might react with NO_3. Although not expected, significant OH fluorescence signals were detected in all measurement cells of the LIF instrument (OH, HO_x, and RO_x in the HO_x and RO_x modes). The signals were equivalent to apparent radical concentrations reaching the order of 1×10^7 cm^{-3} (OH) and 1×10^9 cm^{-3} (HO_x, RO_x) (Fig. 11) and were highly correlated with the mixing ratio of NO_3 (Fig. 12). Notably, the absolute count rates were similar in the OH and HO_x cell. Both cells share the same design and have almost the same OH detection sensitivity. They only differ by additional injection of NO into the air flow in the HO_x cell. Here, unlike in the experiment shown in Fig. 9, the added NO had no influence on the interference signal. The difference in the calculated OH and HO_2 concentrations in Fig. 11 is only due to the different detection sensitivities for OH and HO_2 respectively.

In contrast to the OH and HO_x cell, the NO_3 interference in the RO_x cell gave much higher count rates. In addition, a higher signal was observed in the HO_x mode compared to the RO_x mode. The RO_x mode differs from the HO_x mode by injection of 0.7 ppmv NO into the conversion reactor upstream of the detection cell. In this case, part of the NO_3 was apparently removed by NO, thereby reducing the internal OH production in the RO_x system. Tests with higher NO mixing ratios in the conversion reactor gave even lower OH signals.

The experiment was repeated in a similar way a second time, but OH concentrations were also measured by DOAS. As expected, DOAS measurements did not show any OH. No NO_3 measurements were available during this experiment.

The experiment in SAPHIR with concurrent measurements of the CRDS instrument allowed to quantify the interference from NO_3 in the LIF instrument. In the presence of 10 pptv NO_3 the LIF instrument signals were equivalent to 1.1×10^5 cm^{-3} OH, 1×10^7 cm^{-3} HO_2, and 1.7×10^7 cm^{-3} RO_2. The higher interference for HO_2 compared to OH was due to the lower sensitivity of the HO_2 detection and the higher interference for RO_2 was due to the more efficient conversion of NO_3 in the additional conversion reactor.

5.3 Discussion

Laboratory experiments and experiments in the chamber show that an OH signal is observed in the presence of NO_3. All tests demonstrate that NO_3 is the reason for this signal: (1) the signal can be suppressed by the addition of the NO_3 scavenger NO in laboratory experiments; (2) it correlates with the flow rate through the NO_3/N_2O_5 source in the laboratory test; and (3) it correlates with measurements of NO_3 concentrations by the CRDS instrument in the chamber experiments.

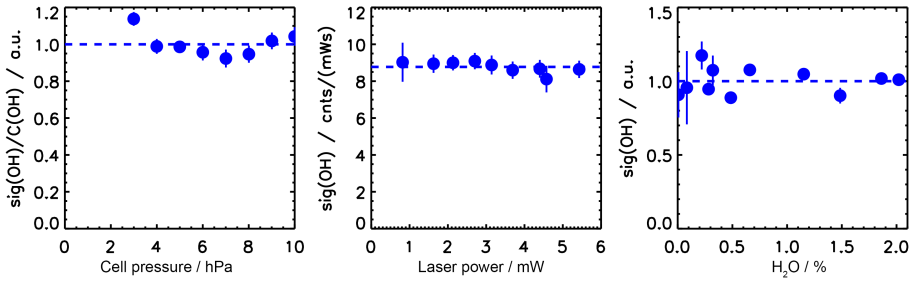

Figure 10. OH signals when air containing NO_3 produced from thermal decomposition of frozen N_2O_5 is sampled depending on the cell pressure, laser power, and water vapour content of the air. No significant change of the signal is observed for either of the parameters. Tests were done with the instrument with the short inlet.

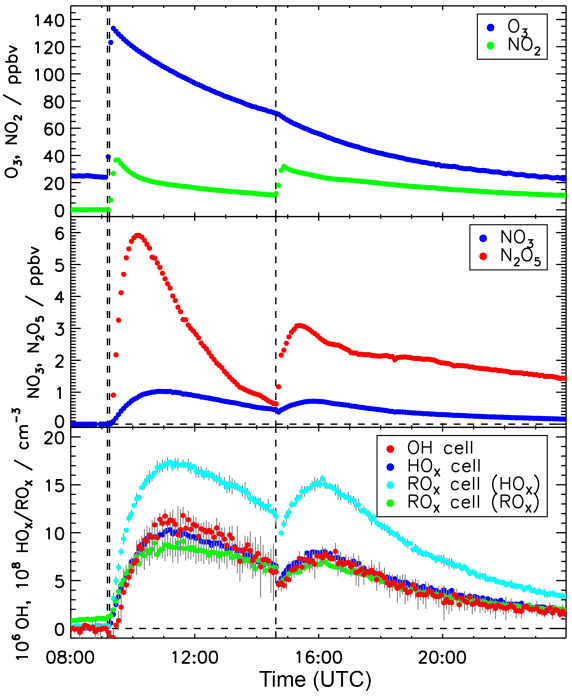

Figure 11. Measured apparent OH, HO_x, and RO_x concentrations (5 min averages) during an experiment in the dark SAPHIR chamber, when only NO_2 and O_3 were injected in dry synthetic air. For differences between OH, HO_x, and RO_x detection, see description of the instrument. NO_3 and N_2O_5 were measured by cavity ring-down spectroscopy. Concentrations in all LIF detection cells (instrument with the short inlet) and measurement modes show similar time series.

The addition of an OH scavenger (CO) upstream of the inlet of the detection chamber has no influence on the OH signal, which suggests that the interference is caused by internal OH production. This conclusion is also supported by the NO_3 experiment in SAPHIR, where the LIF instrument measures an apparent OH concentration of up to 1×10^7 cm^{-3}, while DOAS does not measure concentrations above its limit of detection (0.8×10^6 cm^{-3}).

The OH formation from NO_3 in synthetic air in the measurement cell is difficult to understand. The mechanism must involve a hydrogen-containing compound which reacts either directly with NO_3 or with an NO_3 reaction intermediate. Though the synthetic air is very clean, it may contain traces of water vapour (at the ppmv level) and VOCs (sub pptv) below the detection limit of our instruments. A gas phase reaction with water vapour yielding HNO_3 and OH seems unlikely. It would be highly endothermic ($+71$ kJ mol^{-1}) and can be ruled out, because the interference signal does not change when water vapour is added to the air flow (Fig. 10). Gas phase reactions of NO_3 with VOCs are known to produce peroxy radicals in the atmosphere, but they are unlikely the source of OH in the measurement cell. Given the low concentrations of NO_3 and hypothetical VOC contaminations at the low pressure (4 hPa) in the detection cell, the available reaction time (1.6 ms) would not allow to produce detectable OH concentrations even if the reaction proceeded at gas-kinetic collision rate. Photo-enhanced reactions can also be ruled out, because the internal OH production does not show a dependence on the laser power (Fig. 10).

The OH interference does also not depend on the inlet length of the OH measurement cell (Fig. 9) or the cell pressure (Fig. 10). This suggests that the total residence time of air between the inlet orifice and the laser beam does not play a role. This conclusion is further supported by the observation that the OH and HO_x measurement cells show the same interference signal in SAPHIR chamber experiments (Fig. 12). The HO_x cell differs from the OH cell by injection of NO into the gas expansion about 5 cm downstream of the inlet orifice. The NO concentration is large enough to convert 10 % of HO_2 to OH. Because NO_3 reacts with NO about 3 times faster than HO_2, a complete removal of NO_3 is expected but apparently without effect on the detected interference signal. This suggests that the internal OH is produced in or directly behind the nozzle before the gas flow reaches the NO injection point.

A possible OH production mechanism could be a heterogeneous reaction of NO_3 at a surface of the inlet nozzle, where a layer of H_2O molecules might be adsorbed favoured

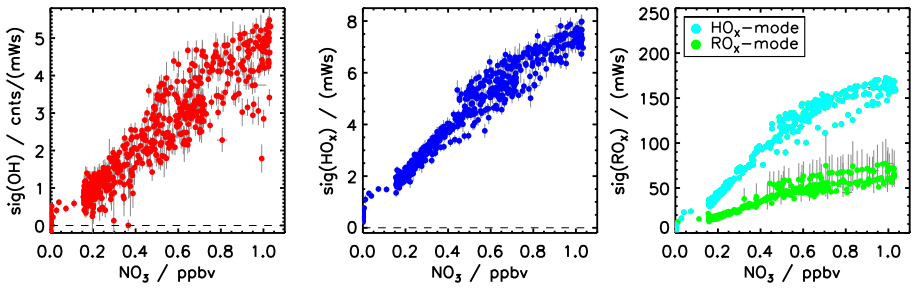

Figure 12. Correlation between count rates in the OH, HO_x, and RO_x cells (HO_x and RO_x mode in the case of the RO_x cell) and measured NO_3 concentrations for the experiment shown in Fig.11.

by the cold gas expansion. NO_3 uptake on pure water was measured by Rudich et al. (1996) and explained by the formation of OH and HNO_3 in the aqueous phase. Largely different rate coefficients were derived for this reaction in different experiments (Rudich et al., 1996; Thomas et al., 1998; Schütze and Herrmann, 2005) without a clear explanation for the discrepancies (Ammann et al., 2013). Schütze and Herrmann (2005) found that the uptake of NO_3 produced equal amounts of gaseous HNO_3, possibly by conversion in a water layer on their reactor walls or catalysed by unknown wall contaminations activated by adsorbed water. It is conceivable that a similar process occurs on the walls of our inlet nozzle and releases OH as a co-product of HNO_3. Another possibility could be the reaction of NO_3 with clusters of gas molecules formed in the cold gas expansion behind the nozzle orifice. Traces of water could be trapped in clusters and react with NO_3, followed by release of OH into the gas phase when the clusters evaporate downstream where the gas is warming up to room temperature. It is, however, difficult to reconcile this explanation with the missing dependence of the interference on the concentration of water vapour (Fig. 10), pointing to a possible saturation effect with respect to the participation of H_2O.

The RO_x measurement system shows a much larger NO_3 interference than the OH and HO_x cells (Fig. 12). The major difference is the RO_x conversion reactor upstream of the detection cell. The converter has a larger nozzle orifice, through which air is sampled. Furthermore, it has a large inner surface and a different wall material (Teflon) (Fuchs et al., 2008b). The residence time of air is approximately 0.6 s at a higher pressure of 25 hPa. Part of the reactor flow is sampled through a second nozzle into the detection cell. In the HO_x mode (only CO is added into the conversion reactor), the interference is a factor of 200 higher than in the other cells. When 0.7 ppmv NO is added (RO_x mode), the interference signal is suppressed by a factor of 2. Under these conditions, the lifetime of NO_3 is only 90 ms and all NO_3 is expected to be removed in the first half of the reactor. The final part of the reactor and the following detection cell are then expected to be free from possible OH production. This could mean that either the surface of the reactor wall contributes to the enhanced interference and/or each of the two nozzle inlets (into the reactor and into the detection cell). Further experimental tests will be needed to explore how NO_3 contributes to the OH production in the gas phase.

Model calculations for the PRIDE-PRD2006 and CARE-BEIJING2006 field campaigns in China 2006 gave maximum NO_3 concentrations of 10 pptv during nighttime. Measured nocturnal OH and HO_2 concentrations, however, were 1×10^6 and 2×10^8 cm^{-3} respectively (Lu et al., 2014), which is much higher than the expected interference from NO_3. During other campaigns in which the Jülich LIF instrument was deployed, no significant OH was measured during nighttime (Holland et al., 1998, 2003).

An interference by NO_3 could be a possible reason for systematic differences between HO_2 measurements reported for dark conditions during the comparison campaign HOx-Comp in 2005 (Fuchs et al., 2010). Good agreement was observed in the sunlit SAPHIR chamber for three LIF HO_x-instruments, when the chamber contained synthetic air, NO_x (up to 300 pptv), and ozone (up to 150 ppbv). When the roof of the chamber was closed, NO_x was quickly removed by the excess of ozone and a significant discrepancy appeared in the HO_2 measurements. After opening the chamber roof, good agreement was reestablished under sunlit conditions. These observations would be consistent with an interference that would be caused by photo-labile NO_3 and emphasize that different instrumental designs could be affected differently by artifacts.

6 Summary and conclusions

Laboratory experiments and experiments in the simulation chamber were conducted in order to test the Jülich OH LIF instruments for interferences from the ozonolysis of alkenes and in the presence of NO_3, which are mostly relevant during nighttime. Concentrations during ozonolysis laboratory experiments with mixing ratios of more than 600 ppbv ozone and up to several ppbv of alkenes were higher than typical concentrations in the atmosphere (Table 1). However, no internal OH production was observed (Fig. 4). Only when exceptionally high reactant concentrations (α-pinene,

limonene, both several ppbv, isoprene, tens of ppbv, propene, ppmv) were used was significant internal OH production observed in laboratory experiments and in chamber experiments (Figs. 5, 8). Overall, we conclude that no significant interference from short-lived products of ozonolysis reactions is expected for atmospheric OH measurements for the Jülich LIF instruments.

The magnitude of the internal OH production that could be observed at exceptionally high reactant concentrations scales with the turnover rate of the ozonolysis reaction in flow tube experiments, where the reaction time was only 1 s. In chamber experiments, much longer timescales (hours) could be tested showing that an internal OH production persisted at a constant level after exposure of the instrument to high reactant concentrations. It is not clear, whether the same mechanism is responsible for the interference on the two timescales. Flow tube experiments demonstrate that internal OH is not produced by photolytic reactions and is independent of the presence of water vapour. The signal does also not change in the presence of SO_2 for the ozonolysis of α-pinene. Stabilized Criegee intermediates that have the potential to decompose in the inlet of LIF OH instruments (Novelli et al., 2014a) are expected to be scavenged in this case (Sipilä et al., 2014), so that this process is unlikely the reason for internal OH production that is observed here. However, internal OH production from the decomposition of sCI species that do not react with SO_2 cannot be excluded.

The Jülich LIF instruments internally produce OH in the presence of NO_3. This was shown in laboratory tests with an NO_3 source and during experiments in the SAPHIR chamber, when NO_3 was produced from the reaction of ozone with NO_2. The exact mechanism behind this interference, however, could not be revealed. Experiments demonstrate that internal OH production occurs directly downstream of the inlet nozzle in the OH and HO_x fluorescence cell and occurs in the RO_x conversion reactor of the RO_x detection system. This points to internal OH production which is possibly caused by surface reactions at chamber walls or reactions with molecular clusters in the gas expansion.

The interference is equivalent to $1.1 \times 10^5\,cm^{-3}$ OH, $1 \times 10^7\,cm^{-3}$ HO_2, and $1.7 \times 10^7\,cm^{-3}$ RO_2 in the presence of 10 pptv NO_3. These numbers suggest that interferences of the Jülich LIF instrument from NO_3 are often negligible for ground-based measurements, when NO_3 concentrations are small. Specifically, measurements of nighttime OH concentrations during the PRIDE-PRD2006 and CAREBEIJING2006 in China 2006 are larger than expected from this interference.

Internal OH production highly depends on the exact design of the instrument. This is demonstrated by the differences in the observed interference from NO_3 between OH/HO_x and RO_x channels. Therefore, it is not clear whether observations of internal OH production reported here can be applied to other instruments.

Acknowledgements. This work was supported by the EU FP-7 program AMIS (Fate and Impact of Atmospheric Pollutants, PIRSES-GA-2011-295132). The authors thank Anna Novelli for useful discussions, Steven Brown, and William Dubé for the support in building the NO_3 instrument and Martin Kaminski for preparing the canisters with organic compounds.

The article processing charges for this open-access publication were covered by a Research Centre of the Helmholtz Association.

Edited by: D. Heard

References

Ammann, M., Cox, R. A., Crowley, J. N., Jenkin, M. E., Mellouki, A., Rossi, M. J., Troe, J., and Wallington, T. J.: Evaluated kinetic and photochemical data for atmospheric chemistry: Volume VI – heterogeneous reactions with liquid substrates, Atmos. Chem. Phys., 13, 8045–8228, doi:10.5194/acp-13-8045-2013, 2013.

Aschmann, S. M., Arey, J., and Atkinson, R.: OH radical formation from the gas-phase reactions of O_3 with a series of terpenes, Atmos. Environ., 36, 4347–4355, doi:10.1016/S1352-2310(02)00355-2, 2002.

Atkinson, R., Baulch, D. L., Cox, R. A., Crowley, J. N., Hampson, R. F., Hynes, R. G., Jenkin, M. E., Rossi, M. J., Troe, J., and IUPAC Subcommittee: Evaluated kinetic and photochemical data for atmospheric chemistry: Volume II – gas phase reactions of organic species, Atmos. Chem. Phys., 6, 3625–4055, doi:10.5194/acp-6-3625-2006, 2006.

Blitz, M. A., Heard, D. E., Pilling, M. J., Arnold, S. R., and Chipperfield, M. P.: Pressure and temperature-dependent quantum yields for the photodissociation of acetone between 279 and 327.5 nm, Geophys. Res. Lett., 31, L06111, doi:10.1029/2003GL018793, 2004.

Broch, S.: Ein neues LIF-Instrument für Flugzeug und Bodengebundene Messungen von OH und HO_2 Radikalen in der Troposphäre, Thesis, 27–48, 2011.

Donahue, N. M., Drozd, G. T., Epstein, S. A., Presto, A. A., and Kroll, J. H.: Adventures in ozoneland: down the rabbit-hole, Phys. Chem. Chem. Phys., 13, 10848–10857, doi:10.1039/C0CP02564J, 2011.

Finlayson-Pitts, B. J. and Pitts Jr., J. N.: Chemistry of the upper and lower atmosphere, Academic Press, San Diego, 179–181, 2000.

Fuchs, H., Dubé, W. P., Ciciora, S. J., and Brown, S. S.: Determination of inlet transmission and conversion efficiencies for in situ measurements of the nocturnal nitrogen oxides, NO_3, N_2O_5 and NO_2, via pulsed cavity ring-down spectroscopy, Anal. Chem., 80, 6010–6017, doi:10.1021/ac8007253, 2008a.

Fuchs, H., Hofzumahaus, A., and Holland, F.: Measurement of tropospheric RO_2 and HO_2 radicals by a laser-induced fluorescence instrument, Rev. Sci. Instrum., 79, 084104, doi:10.1063/1.2968712, 2008b.

Fuchs, H., Dube, W. P., Lerner, B. M., Wagner, N. L., Williams, E. J., and Brown, S. S.: A sensitive and versatile detector for atmospheric NO_2 and NO_X based on blue diode laser cavity ring-down spectroscopy, Environ. Sci. Technol., 43, 7831–7836, doi:10.1021/es902067h, 2009.

Fuchs, H., Brauers, T., Dorn, H.-P., Harder, H., Häseler, R., Hofzumahaus, A., Holland, F., Kanaya, Y., Kajii, Y., Kubistin, D., Lou, S., Martinez, M., Miyamoto, K., Nishida, S., Rudolf, M., Schlosser, E., Wahner, A., Yoshino, A., and Schurath, U.: Technical Note: Formal blind intercomparison of HO_2 measurements in the atmosphere simulation chamber SAPHIR during the HOxComp campaign, Atmos. Chem. Phys., 10, 12233–12250, doi:10.5194/acp-10-12233-2010, 2010.

Fuchs, H., Bohn, B., Hofzumahaus, A., Holland, F., Lu, K. D., Nehr, S., Rohrer, F., and Wahner, A.: Detection of HO_2 by laser-induced fluorescence: calibration and interferences from RO_2 radicals, Atmos. Meas. Tech., 4, 1209–1225, doi:10.5194/amt-4-1209-2011, 2011.

Fuchs, H., Dorn, H.-P., Bachner, M., Bohn, B., Brauers, T., Gomm, S., Hofzumahaus, A., Holland, F., Nehr, S., Rohrer, F., Tillmann, R., and Wahner, A.: Comparison of OH concentration measurements by DOAS and LIF during SAPHIR chamber experiments at high OH reactivity and low NO concentration, Atmos. Meas. Tech., 5, 1611–1626, doi:10.5194/amt-5-1611-2012, 2012.

Griffith, S. M., Hansen, R. F., Dusanter, S., Stevens, P. S., Alaghmand, M., Bertman, S. B., Carroll, M. A., Erickson, M., Galloway, M., Grossberg, N., Hottle, J., Hou, J., Jobson, B. T., Kammrath, A., Keutsch, F. N., Lefer, B. L., Mielke, L. H., O'Brien, A., Shepson, P. B., Thurlow, M., Wallace, W., Zhang, N., and Zhou, X. L.: OH and HO_2 radical chemistry during PROPHET 2008 and CABINEX 2009 – Part 1: Measurements and model comparison, Atmos. Chem. Phys., 13, 5403–5423, doi:10.5194/acp-13-5403-2013, 2013.

Hakola, H., Hellén, H., Hemmilä, M., Rinne, J., and Kulmala, M.: In situ measurements of volatile organic compounds in a boreal forest, Atmos. Chem. Phys., 12, 11665–11678, doi:10.5194/acp-12-11665-2012, 2012.

Hausmann, M., Brandenburger, U., Brauers, T., and Dorn, H.-P.: Detection of tropospheric OH radicals by long-path differential-optical-absorption spectroscopy: Experimental setup, accuracy, and precision, J. Geophys. Res., 102, 16011–16022, doi:10.1029/97jd00931, 1997.

Hens, K., Novelli, A., Martinez, M., Auld, J., Axinte, R., Bohn, B., Fischer, H., Keronen, P., Kubistin, D., Nölscher, A. C., Oswald, R., Paasonen, P., Petäjä, T., Regelin, E., Sander, R., Sinha, V., Sipilä, M., Taraborrelli, D., Tatum Ernest, C., Williams, J., Lelieveld, J., and Harder, H.: Observation and modelling of HO_x radicals in a boreal forest, Atmos. Chem. Phys., 14, 8723–8747, doi:10.5194/acp-14-8723-2014, 2014.

Hofzumahaus, A., Rohrer, F., Lu, K., Bohn, B., Brauers, T., Chang, C.-C., Fuchs, H., Holland, F., Kita, K., Kondo, Y., Li, X., Lou, S., Shao, M., Zeng, L., Wahner, A., and Zhang, Y.: Amplified trace gas removal in the troposphere, Science, 324, 1702–1704, doi:10.1126/science.1164566, 2009.

Holland, F., Hessling, M., and Hofzumahaus, A.: In situ measurement of tropospheric OH radicals by laser-induced fluorescence – a description of the KFA instrument, J. Atmos. Sci., 52, 3393–3401, 1995.

Holland, F., Aschmutat, U., Hessling, M., Hofzumahaus, A., and Ehhalt, D. H.: Highly time resolved measurements of OH during POPCORN using laser-induced fluoresence spectroscopy, J. Atmos. Chem., 31, 205–225, 1998.

Holland, F., Hofzumahaus, A., Schäfer, J., Kraus, A., and Pätz, H. W.: Measurements of OH and HO_2 radical concentrations and photolysis frequencies during BERLIOZ, J. Geophys. Res., 108, 8246, doi:10.1029/2001JD001393, 2003.

Johnson, D. and Marston, G.: The gas-phase ozonolysis of unsaturated volatile organic compounds in the troposphere, Chem. Soc. Rev., 37, 699–716, doi:10.1039/B704260B, 2008.

Lee, Y.-P.: Perspective: Spectroscopy and kinetics of small gaseous Criegee intermediates, J. Chem. Phys., 143, 020901, doi:10.1063/1.4923165, 2015.

Li, X., Rohrer, F., Hofzumahaus, A., Brauers, T., Häseler, R., Bohn, B., Broch, S., Fuchs, H., Gomm, S., Holland, F., Jäger, J., Kaiser, J., Keutsch, F. N., Lohse, I., Lu, K., Tillmann, R., Wegener, R., Wolfe, G. M., Mentel, T. F., Kiendler-Scharr, A., and Wahner, A.: Missing gas-phase source of HONO inferred from Zeppelin measurements in the troposphere, Science, 344, 292–296, doi:10.1126/science.1248999, 2014.

Lu, K. D., Rohrer, F., Holland, F., Fuchs, H., Bohn, B., Brauers, T., Chang, C. C., Häseler, R., Hu, M., Kita, K., Kondo, Y., Li, X., Lou, S. R., Nehr, S., Shao, M., Zeng, L. M., Wahner, A., Zhang, Y. H., and Hofzumahaus, A.: Observation and modelling of OH and HO_2 concentrations in the Pearl River Delta 2006: a missing OH source in a VOC rich atmosphere, Atmos. Chem. Phys., 12, 1541–1569, doi:10.5194/acp-12-1541-2012, 2012.

Lu, K. D., Hofzumahaus, A., Holland, F., Bohn, B., Brauers, T., Fuchs, H., Hu, M., Häseler, R., Kita, K., Kondo, Y., Li, X., Lou, S. R., Oebel, A., Shao, M., Zeng, L. M., Wahner, A., Zhu, T., Zhang, Y. H., and Rohrer, F.: Missing OH source in a suburban environment near Beijing: observed and modelled OH and HO_2 concentrations in summer 2006, Atmos. Chem. Phys., 13, 1057–1080, doi:10.5194/acp-13-1057-2013, 2013.

Lu, K. D., Rohrer, F., Holland, F., Fuchs, H., Brauers, T., Oebel, A., Dlugi, R., Hu, M., Li, X., Lou, S. R., Shao, M., Zhu, T., Wahner, A., Zhang, Y. H., and Hofzumahaus, A.: Nighttime observation and chemistry of HO_x in the Pearl River Delta and Beijing in summer 2006, Atmos. Chem. Phys., 14, 4979–4999, doi:10.5194/acp-14-4979-2014, 2014.

Mao, J., Ren, X., Zhang, L., Van Duin, D. M., Cohen, R. C., Park, J.-H., Goldstein, A. H., Paulot, F., Beaver, M. R., Crounse, J. D., Wennberg, P. O., DiGangi, J. P., Henry, S. B., Keutsch, F. N., Park, C., Schade, G. W., Wolfe, G. M., Thornton, J. A., and Brune, W. H.: Insights into hydroxyl measurements and atmospheric oxidation in a California forest, Atmos. Chem. Phys., 12, 8009–8020, doi:10.5194/acp-12-8009-2012, 2012.

Mauldin III, R. L., Berndt, T., Sipila, M., Paasonen, P., Petaja, T., Kim, S., Kurten, T., Stratmann, F., Kerminen, V. M., and Kulmala, M.: A new atmospherically relevant oxidant of sulphur dioxide, Nature, 488, 193–196, doi:10.1038/nature11278, 2012.

MCM: Master Chemical Mechanism, available at: http://mcm.leeds.ac.uk/MCM/, 2012.

Monks, P. S., Granier, C., Fuzzi, S., Stohl, A., Williams, M. L., Akimoto, H., Amann, M., Baklanov, A., Baltensperger, U., Bey, I., Blake, N., Blake, R. S., Carslaw, K., Cooper, O. R., Dentener, F., Fowler, D., Fragkou, E., Frost, G. J., Generoso, S., Ginoux, P., Grewe, V., Guenther, A., Hansson, H. C., Henne, S., Hjorth, J., Hofzumahaus, A., Huntrieser, H., Isaksen, I. S. A., Jenkin, M. E., Kaiser, J., Kanakidou, M., Klimont, Z., Kulmala, M., Laj, P., Lawrence, M. G., Lee, J. D., Liousse, C., Maione, M., McFiggans, G., Metzger, A., Mieville, A., Moussiopoulos, N., Orlando, J. J., O'Dowd, C. D., Palmer, P. I., Parrish, D. D., Petzold, A., Platt, U., Pöschl, U., Prevot, A. S. H., Reeves, C. E., Reimann,

S., Rudich, Y., Sellegri, K., Steinbrecher, R., Simpson, D., ten Brink, H., Theloke, J., van der Werf, G. R., Vautard, R., Vestreng, V., Vlachokostas, C., and von Glasow, R.: Atmospheric composition change – global and regional air quality, Atmos. Environ., 43, 5268–5350, doi:10.1016/j.atmosenv.2009.08.021, 2009.

Newland, M. J., Rickard, A. R., Alam, M. S., Vereecken, L., Munoz, A., Rodenas, M., and Bloss, W. J.: Kinetics of stabilised Criegee intermediates derived from alkene ozonolysis: reactions with SO_2, H_2O and decomposition under boundary layer conditions, Phys. Chem. Chem. Phys., 17, 4076–4088, doi:10.1039/C4CP04186K, 2015a.

Newland, M. J., Rickard, A. R., Vereecken, L., Muñoz, A., Ródenas, M., and Bloss, W. J.: Atmospheric isoprene ozonolysis: impacts of stabilised Criegee intermediate reactions with SO_2, H_2O and dimethyl sulfide, Atmos. Chem. Phys., 15, 9521–9536, doi:10.5194/acp-15-9521-2015, 2015b.

Novelli, A., Hens, K., Tatum Ernest, C., Kubistin, D., Regelin, E., Elste, T., Plass-Dülmer, C., Martinez, M., Lelieveld, J., and Harder, H.: Characterisation of an inlet pre-injector laser-induced fluorescence instrument for the measurement of atmospheric hydroxyl radicals, Atmos. Meas. Tech., 7, 3413–3430, doi:10.5194/amt-7-3413-2014, 2014a.

Novelli, A., Vereecken, L., Lelieveld, J., and Harder, H.: Direct observation of OH formation from stabilised Criegee intermediates, Phys. Chem. Chem. Phys., 16, 19941–19951, doi:10.1039/C4CP02719A, 2014b.

Peeters, J., Müller, J.-F., Stavrakou, T., and Nguyen, V. S.: Hydroxyl radical recycling in isoprene oxidation driven by hydrogen bonding and hydrogen tunneling: The upgraded LIM1 mechanism, J. Phys. Chem. A, 118, 8625–8643, doi:10.1021/jp5033146, 2014.

Ren, X., Harder, H., Martinez, M., Falona, I. C., Tan, D., Lesher, R. L., di Carlo, P., Simpas, J. B., and Brune, W. H.: Interference testing for atmospheric HO_X measurements by laser-induced fluorescence, J. Atmos. Chem., 47, 169–190, doi:10.1023/B:JOCH.0000021037.46866.81, 2004.

Rohrer, F., Lu, K., Hofzumahaus, A., Bohn, B., Brauers, T., Chang, C.-C., Fuchs, H., Häseler, R., Holland, F., Hu, M., Kita, K., Kondo, Y., Li, X., Lou, S., Oebel, A., Shao, M., Zeng, L., Zhu, T., Zhang, Y., and Wahner, A.: Maximum efficiency in the hydroxyl-radical-based self-cleansing of the troposphere, Nat. Geosci., 7, 559–563, doi:10.1038/ngeo2199, 2014.

Rudich, Y., Talukdar, R. K., Ravishankara, A. R., and Fox, R. W.: Reactive uptake of NO_3 on pure water and ionic solutions, J. Geophys. Res., 101, 21023–21031, doi:10.1029/96JD01844, 1996.

Schlosser, E., Bohn, B., Brauers, T., Dorn, H.-P., Fuchs, H., Häseler, R., Hofzumahaus, A., Holland, F., Rohrer, F., Rupp, L. O., Siese, M., Tillmann, R., and Wahner, A.: Intercomparison of two hydroxyl radical measurement techniques at the atmosphere simulation chamber SAPHIR, J. Atmos. Chem., 56, 187–205, doi:10.1007/s10874-006-9049-3, 2007.

Schlosser, E., Brauers, T., Dorn, H.-P., Fuchs, H., Häseler, R., Hofzumahaus, A., Holland, F., Wahner, A., Kanaya, Y., Kajii, Y., Miyamoto, K., Nishida, S., Watanabe, K., Yoshino, A., Kubistin, D., Martinez, M., Rudolf, M., Harder, H., Berresheim, H., Elste, T., Plass-Dülmer, C., Stange, G., and Schurath, U.: Technical Note: Formal blind intercomparison of OH measurements: results from the international campaign HOxComp, Atmos. Chem. Phys., 9, 7923–7948, doi:10.5194/acp-9-7923-2009, 2009.

Schütze, M. and Herrmann, H.: Uptake of the NO_3 radical on aqueous surfaces, J. Atmos. Chem., 52, 1–18, doi:10.1007/s10874-005-6153-8, 2005.

Sipilä, M., Jokinen, T., Berndt, T., Richters, S., Makkonen, R., Donahue, N. M., Mauldin III, R. L., Kurtén, T., Paasonen, P., Sarnela, N., Ehn, M., Junninen, H., Rissanen, M. P., Thornton, J., Stratmann, F., Herrmann, H., Worsnop, D. R., Kulmala, M., Kerminen, V.-M., and Petäjä, T.: Reactivity of stabilized Criegee intermediates (sCIs) from isoprene and monoterpene ozonolysis toward SO2 and organic acids, Atmos. Chem. Phys., 14, 12143–12153, doi:10.5194/acp-14-12143-2014, 2014.

Taatjes, C. A., Shallcross, D. E., and Percival, C. J.: Research frontiers in the chemistry of Criegee intermediates and tropospheric ozonolysis, Phys. Chem. Chem. Phys., 16, 1704–1718, doi:10.1039/C3CP52842A, 2014.

Thomas, K., Volz-Thomas, A., Mihelcic, D., Smit, H. G. J., and Kley, D.: On the exchange of NO_3 radicals with aqueous solutions: solubility and sticking coefficient, J. Atmos. Chem., 29, 17–43, doi:10.1023/A:1005860312363, 1998.

Vereecken, L., Harder, H., and Novelli, A.: The reaction of Criegee intermediates with NO, RO_2, and SO_2, and their fate in the atmosphere, Phys. Chem. Chem. Phys., 14, 14682–14695, doi:10.1039/C2CP42300F, 2012.

Vereecken, L., Harder, H., and Novelli, A.: The reactions of Criegee intermediates with alkenes, ozone, and carbonyl oxides, Phys. Chem. Chem. Phys., 16, 4039–4049, doi:10.1039/C3CP54514H, 2014.

Wagner, N. L., Dubé, W. P., Washenfelder, R. A., Young, C. J., Pollack, I. B., Ryerson, T. B., and Brown, S. S.: Diode laser-based cavity ring-down instrument for NO_3, N_2O_5, NO, NO_2 and O_3 from aircraft, Atmos. Meas. Tech., 4, 1227–1240, doi:10.5194/amt-4-1227-2011, 2011.

Yuan, B., Veres, P. R., Warneke, C., Roberts, J. M., Gilman, J. B., Koss, A., Edwards, P. M., Graus, M., Kuster, W. C., Li, S.-M., Wild, R. J., Brown, S. S., Dubé, W. P., Lerner, B. M., Williams, E. J., Johnson, J. E., Quinn, P. K., Bates, T. S., Lefer, B., Hayes, P. L., Jimenez, J. L., Weber, R. J., Zamora, R., Ervens, B., Millet, D. B., Rappenglück, B., and de Gouw, J. A.: Investigation of secondary formation of formic acid: urban environment vs. oil and gas producing region, Atmos. Chem. Phys., 15, 1975–1993, doi:10.5194/acp-15-1975-2015, 2015.